Urban Climate 38 (2021) 100911

Contents lists available at ScienceDirect

Urban Climate

journal homepage: www.elsevier.com/locate/uclim

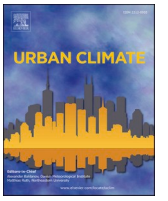

Spatial modeling of rainfall patterns and groundwater on the coast of northeastern Brazil

Marcos Vinícius da Silva [a,*], Héliton Pandorfi [a], Alexandre Maniçoba da Rosa Ferraz Jardim [a,b], José Francisco de Oliveira-Júnior [c], Jesiele Silva da Divincula [a], Pedro Rogerio Giongo [d], Thieres George Freire da Silva [a,b], Gledson Luiz Pontes de Almeida [a], Geber Barbosa de Albuquerque Moura [a], Pabricio Marcos Oliveira Lopes [a,e]

[a] *Department of Agricultural Engineering, Federal Rural University of Pernambuco, Dom Manoel de Medeiros avenue, s/n, Dois Irmãos, Recife, Pernambuco 52171-900, Brazil*
[b] *Postgraduate Program in Plant Production, Academic Unit of Serra Talhada, Federal Rural University of Pernambuco, Gregório Ferraz Nogueira avenue, s/n, Serra Talhada, Pernambuco 56909-535, Brazil*
[c] *Laboratório de Meteorologia Aplicada e Meio Ambiente (LAMMA), Institute of Atmospheric Sciences (ICAT), Federal University of Alagoas (UFAL), Maceió, Alagoas 57072-260, Brazil*
[d] *Department of Agricultural Engineering, State University of Goiás, Via Protestato Joaquim Bueno, 945, Perímetro Urbano, 75920-000, Santa Helena de Goiás, Goiás, Brazil*
[e] *Department of Agronomy, Federal Rural University of Pernambuco, Dom Manoel de Medeiros avenue, SN, Dois Irmãos, Recife, Pernambuco 52171-900, Brazil*

ARTICLE INFO

Keywords:
Rainfall
Urban centers
Meteorological data
Geostatistics
Kriging maps

ABSTRACT

The objective of this study was to characterize the patterns of monthly rainfall in the mesoregions of Zona da Mata and Metropolitan of Recife in the state of Pernambuco, Brazil, based on geostatistical techniques and multivariate analysis, in addition to establishing rain flow strategies in urban centers and alerting of possible impacts on local aquifers. The meteorological data are from a 20-year time series (2000–2019). Maps of the projection of aquifers, hydrochemical and hydrogeological for the study region were established. The pluviometric data were submitted to descriptive, geostatistical, and multivariate analysis. The Gaussian model was the one that best fitted ($R^2 \geq 0.84$). The Atlantic interhemispheric sea surface temperature gradient together with Easterly Wave Disturbances, Intertropical Convergence Zone, sea breezes circulations, and trade winds interfered in the dynamics of coastal rains, especially on the Northeast Brazilian coast. The hydrogeological formation of groundwater on the coast, of the porous type, justified the higher flows of groundwater associated with the greater rainfall. Kriging maps were consistent in the spatialization of rains on the coast of Pernambuco and, thus, making it possible to assess the dynamics of rains and the creation of socio-economic strategies, to minimize the impacts during the period of heavy rains and major floods.

* Corresponding author.
E-mail addresses: marcolino_114@hotmail.com (M.V. Silva), heliton.pandorfi@ufrpe.br (H. Pandorfi), alexandremrfj@gmail.com (A.M.R.F. Jardim), jose.junior@icat.ufal.br (J.F. Oliveira-Júnior), jeeh.divincula@gmail.com (J.S. Divincula), pedro.giongo@ueg.br (P.R. Giongo), thieres.silva@ufrpe.br (T.G.F. Silva), gledson@deagri.ufrpe.br (G.L.P. Almeida), geber.moura@ufrpe.br (G.B.A. Moura), pabriciope@gmail.com (P.M.O. Lopes).

https://doi.org/10.1016/j.uclim.2021.100911
Received 19 February 2021; Received in revised form 10 June 2021; Accepted 30 June 2021
Available online 3 July 2021

1. Introduction

Population growth associated with urban density has exposed the world population to extreme climates (e.g., storms, flash floods, prolonged droughts, and severe droughts). The aforementioned combined factors interfere with the variability of rainfall and, therefore, a better understanding and representation in the search for strategies that are essential for the local population is necessary (Courty et al., 2018; Sivakumar et al., 2019; Dai et al., 2020).

The relationship between rainfall and atmospheric circulation, together with its spatio-temporal variability, has been widely studied in large urban centers (Ramos et al., 2014; Gois et al., 2020; Lima et al., 2021) and in megacities (Baklanov et al., 2016). The analysis of rainfall patterns is essential to establish strategies in the management of agricultural, environmental risk, and large urban centers, such as urban infrastructure, urban erosivity, generation of sediments from rainwater courses, among others (Haris et al., 2017; Jardim et al., 2017; Sivakumar et al., 2019; Peña-Angulo et al., 2020; Terassi et al., 2020).

Therefore, understanding how the movement of rains works and how they interact with the urban environment both in space and in time is essential (Yilmaz et al., 2016; Jardim et al., 2019; Costa et al., 2021), especially in Brazil, where there are occurrences of waterborne diseases (dengue and leptospirosis) that affect the population, mainly in Northeast Brazil (NEB) - (Santos et al., 2018; Oliveira-Júnior et al., 2019). The development of a reliable approach to adequately describe the movement of rainfall is recognized as a challenging task in the world and, especially in Brazil.

Recent research has shown satisfactory and promising results with the use of geostatistical techniques in the spatio-temporal representation of rainfall, for example, the kriging interpolation method highlights rainfall patterns and provides a detailed visual analysis of the sectors with the highest and lowest occurrence of rainfall (Gois et al., 2015; Arowolo et al., 2017; Javari, 2017a; Medeiros et al., 2019; Vessia et al., 2020).

Among the statistical techniques used to investigate the spatio-temporal variations of meteorological variables, the cluster analysis (decision tree classifier - DTC) for delimiting homogeneous regions and identifying regional and global climatic patterns has increased in recent years (Lyra et al., 2014; Silva et al., 2018; Santos et al., 2019; Silva et al., 2020a). The relevance of this technique is related not only to the quality and types of variables that can be grouped in different aspects but also to the identification of similarity and dissimilarity patterns between the study variables (Tobar and Wyseure, 2017; Rahman et al., 2018).

Thus, due to the flexibility of the combinations of methods and similarity metrics, the hierarchical cluster analysis is suitable for different purposes and situations, which makes its application comprehensive and effective for different types of variables and studies.

With just over 5 million inhabitants, the mesoregions of Zona da Mata and the Recife Metropolitan Region are among the most populous regions of Brazil (IBGE, 2020a). In both places show annual rainfall of more than 2000 mm, being one of the urban regions with the highest rainfall in northeastern Brazil (APAC, 2020).

Given the high rate of urbanization, mainly in the metropolitan mesoregion of Recife, every year they face flooding problems, caused by the rainy season (Nóbrega et al., 2015). Because of this scenario, studying rainfall patterns in this region becomes fundamental and essential to establish management strategies in urban centers. Thus, to fill the knowledge gaps in existing studies, based on the above, the objective of this research was to characterize the monthly rainfall patterns in the mesoregions of Zona da Mata and Metropolitan of Recife in the state of Pernambuco, Brazil, based on techniques geostatistics and multivariate analysis, in addition to establishing the patterns of rainfall in urban centers and warning of possible impacts on local aquifers.

2. Material and methods

2.1. Characterization of the study area

The study was carried out in the mesoregions of Zona da Mata and Metropolitan of Recife in the state of Pernambuco (PE) - Brazil, which comprise the coastal region of the state and are located in the parallels of 7°24′S and 8°53′S and, the meridians 34°30′W and 36°20′W. According to the Köppen-Geiger climate classification, the studied mesoregions are found in two climatic zones: “Am”—humid or sub-humid tropical climate, and “Aw”—tropical climate with a dry winter season (Fig. 1) - (Alvares et al., 2013; Beck et al., 2018).

The mesoregion of Zona da Mata of Pernambuco is formed by 43 municipalities and has an estimated population of 1,388,810 inhabitants, according to the Brazilian Institute of Geography and Statistics (IBGE) - (IBGE, 2020a). With a territorial extension of 8401.437 km^2, demographic density of 7275.050 inhabitants km^{-2}. The mesoregion Metropolitan of Recife consists of 15 municipalities and has an estimated population of 4,026,826 inhabitants (IBGE, 2020a). With a territorial extension of 2780.120 km^2 and a demographic density of 27,821.660 inhabitants km^{-2}. Both mesoregions are crossed by three main rivers, Ipanema, Capibaribe, and Ipojuca, under the domain of the Atlantic Forest biome (IBGE, 2020a). The mesoregions of Zona da Mata and Metropolitan of Recife comprise the coastal region of the state of PE.

2.2. Weather stations and fault filling

A network of 39 weather stations from the Pernambuco Water and Climate Agency (APAC[1]) platform were used, from a monthly

[1] http://old.apac.pe.gov.br/meteorologia/monitoramento-pluvio.php

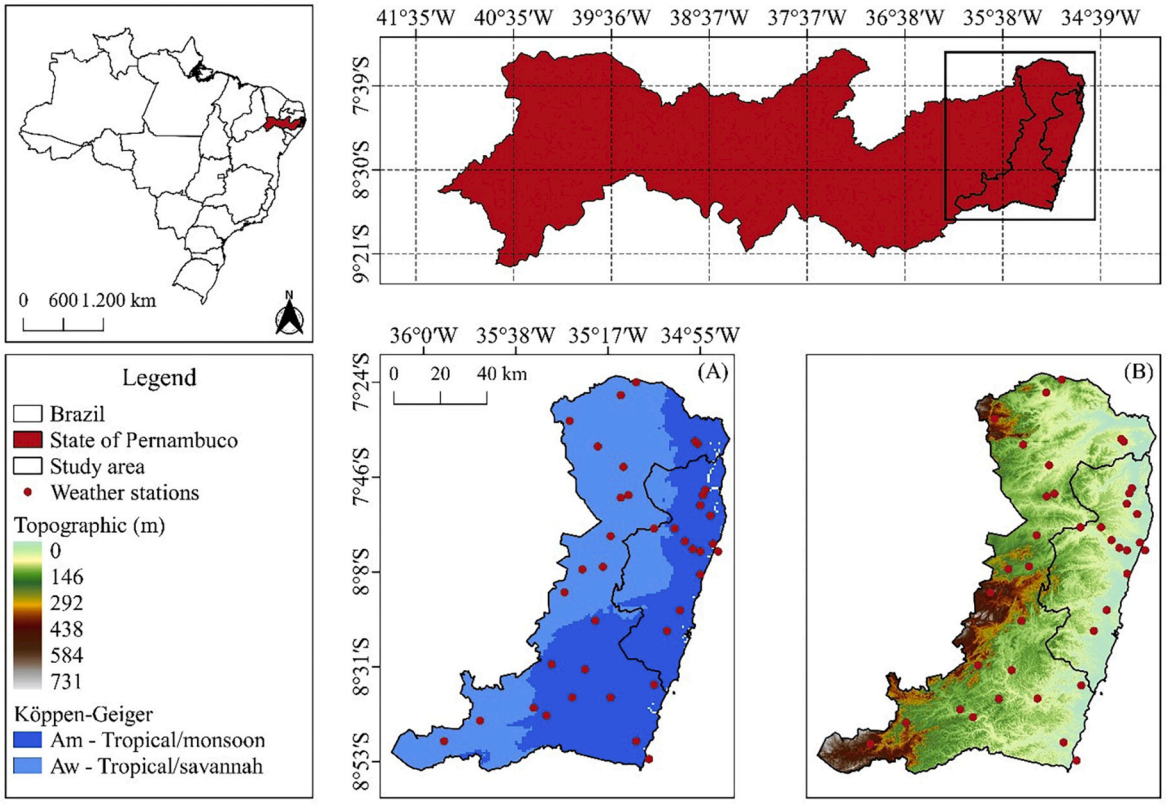

Fig. 1. Location of the study area, followed by the weather stations, climatic zones (Aw and Am), according to the Köppen-Geiger climate classification (A) and digital elevation (m) based on Shuttle Radar Topography Mission (SRTM) data (B).

time series from 2000 to 2019. The filling of the gaps was performed based on the simple linear regression model (SLRM) used to fill in gaps (Thom, 1966; Kite, 1988; Serra et al., 2016) and, being used in the scientific literature with satisfactory results to the East of the Northeast (ENEB) (Lyra et al., 2014; Lyra et al., 2017) and other regions of Brazil (Brito et al., 2017; Silva et al., 2020b) and world (Kamruzzaman et al., 2011; Kamruzzaman et al., 2017; Uele et al., 2017). It was found that most stations have less than 20% of missing data across the imputation series.

2.3. Characterization of aquifers, hydrogeology, and groundwater hydrochemistry in the study area

A map of the aquifer projection in the study region was established. The mapping of the Outcropping Areas of Aquifers and Aquifer Systems in Brazil, on a scale of 1:1,000,000, was produced by the Groundwater Management (GESUB) of the National Water Agency (ANA) based on the Geological Map of Brazil to the Millionth (CPRM), state geological maps, in scales between 1:500,000 and 1:1,000,000, Map of Hydrogeological Domains and Subdomains of Brazil, cut 1:1,000,000 and information 1:2,500,000. The data are available in the shapefile format on the National Spatial Data Infrastructure platform (INDE, 2013). Based on the database made available by IBGE, a hydrogeological (IBGE, 2018) and hydrochemical (IBGE, 2020b) map of the study region was generated.

The Hydrogeological Map of the Northeast Region of Brazil cartographically represents the productivity of aquifers in this region based on the values of flows and specific flows of 54,864 tubular wells. This information is stored in a database and grouped at intervals. This database follows, in part, the procedures used in the Map of Hydrogeological Domains/Subdomains of Brazil and the Hydrogeological Charters of Brazil to the Millionth (CPRM, 2007).

The Groundwater Hydrochemistry Map of the Northeast Region of Brazil brings together a collection of 10,478 physical-chemical analyzes, all coming from tubular wells and chemically homogeneous domains concerning potability, chemical facies, and the suitability of water for use in irrigation. The chemical reports were incorporated into a database (prepared in Access) and classified using applications. These determinations were migrated and georeferenced in GeoMedia, where work was carried out to individualize chemically homogeneous zones, using geological, physiographic, and hydrogeological criteria that allowed the demarcation of units that have more or less similar characteristics within their limits.

The data made available on the platform are in vector format (.shp), with an established pre-classification, in which geoprocessing techniques were applied to reclassify these vectors to the area comprising the study, using the "categorized classification" tool of QGis 3.12 software (QGIS Development Team, 2020).

2.4. Boxplot analysis

A boxplot analysis was performed to identify outliers and statistical properties, that is, three percentiles (median and interquartile range) and the minimum and maximum values (whisker, represented by the lines of the standard boxplot), constituting the so-called summary of five numbers, of the 20-year series weather stations used in the study (Fig. 2A and B). This type of analysis of climatological consistency supports the signaling of suspicious values (Lima et al., 2021).

2.5. Statistical analysis

The temporal variability data were submitted to descriptive statistical analysis to obtain the mean, median, minimum, maximum, standard deviation, coefficient of variation (CV, %), asymmetry, and kurtosis. The percentage value of the CV was categorized as low (CV < 12%); medium (if CV = 12–24%) and high (when CV > 24%) - (Warrick and Nielsen, 1980), subsequently, the Kolmogorov-Smirnov (KS) normality test was also applied, using a significance level of $p \leq 0.01$. The data submitted to descriptive statistics were related to a general average of the study area, in which the average rainfall in the study region was characterized.

To elucidate the spatial trend, we used geostatistical analysis based on the calculation of classic semivariances, based on Eq. (1), which estimated the spatial structure and dependence between the pairs of observations.

$$\gamma(h) = \frac{1}{2N(h)} \sum_{i=1}^{N(h)} [Z(X_i) - Z(X_i + h)]^2 \quad (1)$$

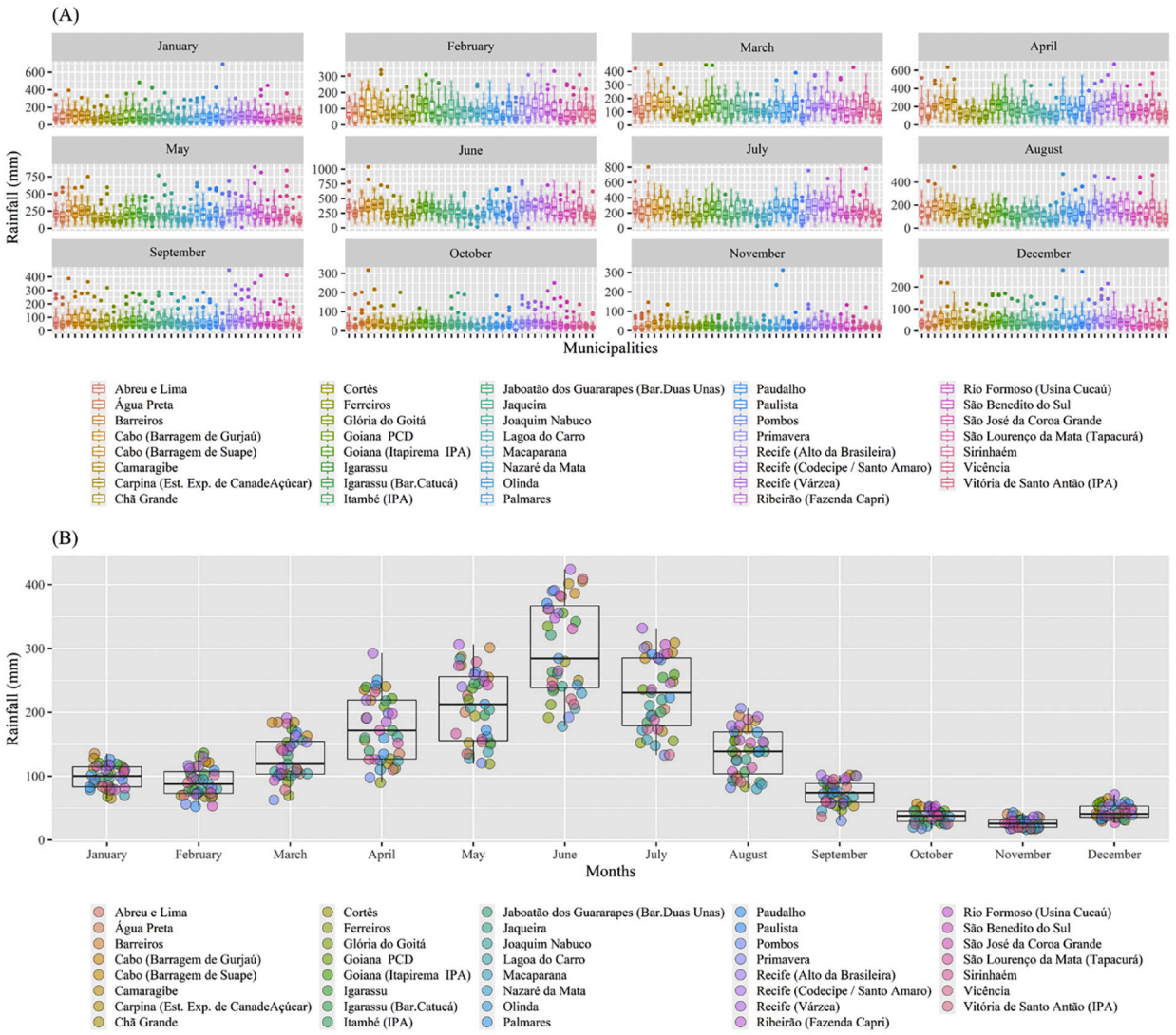

Fig. 2. Boxplot of the annual rainfall of the weather stations over the months (A) overview of the monthly boxplots of the 20-year series (B).

where, γ(h) - is the experimental semi-variance estimator, obtained by the sampled values $Z(X_i)$, $Z(X_i + h)$; N(h) - is the number of measured value pairs separated by the vector or delay distance; h - is the distance between sample pairs (i.e., it is the distance between two samples); and $Z(X_i)$ and $Z(X_i + h)$ - are the values of the *i*-th observation of the regionalized variable, collected at points X_i and $X_i + h$ ($i = 1, \ldots, n$), separated by the vector h.

Spatial dependence was analyzed by adjusting the semivariogram based on the estimate of the semivariance using the GEO-EAS® program (England et al., 1989). The data were adjusted to the Spherical, Exponential, and Gaussian models Eqs. (2), (3), and (4), respectively, according to Deutsch and Journel (1998).

Spherical Model:

$$\gamma(h) = \begin{cases} C_0 + C \cdot \left[1.5\frac{h}{a} - 0.5\left(\frac{h}{a}\right)^3\right], & \text{for } 0 \le h \le a \\ C_0 + C, & \text{for } h > a \end{cases} \quad (2)$$

Exponential Model:

$$\gamma(h) = C_0 + C.\left[1 - exp\left(-\frac{3h}{a}\right)\right] \quad (3)$$

Gaussian model:

$$\gamma(h) = C_0 + C \cdot \left[1 - exp\left(-\frac{(3h)^2}{a^2}\right)\right] \quad (4)$$

where, γ(h) - is the experimental semi-variance estimator; $C_0 + C$ - is the sill (i.e., it is the nugget effect plus the variance dispersion, given by the acronyms C_0 and C, respectively); h - is the distance between sample pairs; *a* - is the range (m). Such variables are key factors in describing the overall structure, as well as the inputs used for interpolation.

The adjusted semivariograms were submitted to Jack-Knifing cross-validation, in which the mean must be close to zero and the standard deviation close to 1.0 (Vauclin et al., 1983), the program used for this analysis was the GEO-EAS® (England et al., 1989). The degree of spatial dependence (DSD) was classified according to Cambardella et al. (1994), which suggests strong dependence (St) < 25%; moderate dependence (Md) between 25 and 75%; and weak dependence (We) > 75%. For making the kriging maps, the Surfer 9 program (Golden Software, 2010) was used. Cross-validation by Jack-Knifing is essential for the reliability of the semivariogram (Silva et al., 2019; Lopes et al., 2020; Silva et al., 2020c).

To determine the similarity between the months of the year and between the weather stations in the study area, the cluster analysis technique was applied via dendrogram, using the Ward method and based on the Euclidean distance (Ward, 1963; Lyra et al., 2014). The similarities were attributed to the months of the year by calculating the Euclidean distance (d_{ij}) and by Ward's hierarchical method (indicated for analysis of climatic data) between two objects (*i* and *j*), in which, the shorter their distance, the greater the quantitative similarity between individuals (Ward, 1963; Lyra et al., 2014), as described in Eqs. (5) and (6), respectively.

$$d_{ij} = \sqrt{\sum_{k=1}^{n} \left(x_{ik} - x_{jk}\right)^2} \quad (5)$$

where, d_{ij} - Euclidean distance; and x_{ik} and x_{jk} - data observed at the weather stations of municipalities *i* and *j*, respectively.

$$W = \left[\sum_{i=1}^{n} x_i^2 - \frac{1}{n}\left(\sum x_i\right)^2\right] \quad (6)$$

where, W - minimum intergroup variance by Ward's hierarchical method; *n* - number of elements; and x_i - an *i*-th member of the group.

The cluster analysis was calculated using RStudio version 3.6.1 (R Core Team, 2019). From the groups formed by the weather stations, they were spatialized in the form of maps, to verify the patterns of rainfall distribution. To generate the maps, processing was performed using QGis v. 3.12 (QGIS Development Team, 2020).

3. Results and discussion

3.1. Descriptive and geostatistical analysis of rainfall

Table 1 presents descriptive statistics for the months from January to December, based on a general average in the time series of the meteorological stations used in the study. According to the criteria of Warrick and Nielsen (1980), the CV% was high (CV% > 24%) for all the months evaluated, except January. Rainfall has high spatial variability, depending on abiotic factors (e.g., temperature, air humidity, evapotranspiration, wind speed, air masses, and others), tending to a high CV%.

Similar results were obtained by Javari (2017b), who analyzed the spatial variability of monthly precipitation trends in Iran and

observed a high CV% for rainfall data, the characteristic and direct influence of abiotic factors. Wodaje et al. (2016) studied the spatio-temporal variability of the distribution of rainfall along the altitudinal gradient in the Bilate river basin, Southern Ethiopia, and observed variations in CV% from medium to high.

All evaluated months presented normal data for the KS test. For data normality, the mean and median must be close, a factor verified for all months of the year (Table 1). Gois et al. (2020), applied statistical normality tests and homogeneity of a data set of rainfall of 71 years for the state of Rio de Janeiro, the applied tests did not present normality for the unfilled data, as well as for a fraction of the filled data. However, it is noteworthy that in the descriptive analysis of the data, the means and medians showed distant values, differing from the present study.

The geostatistical models evaluated in the study based on the nugget effect, sill, and range are shown in Table 2. For all the months evaluated, the Gaussian model presented the best fit, therefore, recommended for studies of spatial variability of rainfall for the study area. The determination coefficient (R^2) showed a satisfactory adjustment, with values greater than 0.84, for all months of the year.

The results obtained corroborate the responses reached by Sarangi et al. (2005) who applied geostatistical methods to predict the spatial variability of rainfall in a mountainous region of Santa Lucia Island in the Caribbean, where they obtained an R^2 greater than 0.9, for all months of the year, differing only regarding the semivariogram model adjusted, which in this case was spherical. Unlike Gois et al. (2015), who applied transitive theoretical models in episodes of El Niño Strong, based on data obtained from the SPI (Standardized Precipitation Index), for the state of Tocantins - Brazil, which highlighted the spherical and exponential models for identifying events drought satisfactorily.

The degree of spatial dependence (DSD) was significant for all the months evaluated (Table 2) and describes the intensity between the collection points, showing a strong dependency pattern, which indicates that the representation of spatial variability is highly accurate.

The nugget effect (C_0) for all the months studied was greater than 1.0 (one), which denotes little measurement accuracy (Cambardella et al., 1994), except for the month of November, when C_0 was less than 1.0 (one). However, the low precision for C_0 is normal, since precipitation data show high spatial variability observed by the high CV% (Table 1).

The semivariogram models for all months were subjected to cross-validation by Jack-Knifing, with a mean close to 0 and a standard deviation close to 1 (Vauclin et al., 1983) - (Table 2). Corroborating the findings of the present study, Sarangi et al. (2005), using the similar methodology of cross-validation, with the kriged average error (KAE) was close to 0 and the kriged reduced mean square error (KRMSE) close to 1 (Campling et al., 2001; Kitanidis, 1997) for rainfall data throughout the year, presenting satisfactory validation for semivariograms.

3.2. Rainfall kriging maps

Based on the established and validated semivariogram models, kriging maps for the spatio-temporal distribution of rainfall for the Pernambuco coast were made (Fig. 3). The highest rainfall records occurred in the coastal region, with the period from April to August being the wettest months. However, despite this rainy period, rains >30 mm were recorded in the study region throughout the year, except for October to December, with rains <30 mm (Table 1 and Fig. 3). The variability of rainfall corroborates the results obtained by Nóbrega et al. (2015), in which the spatial-temporal variability of rainfall in PE occurred from March to August, with higher rainfall records.

Between the months of January to March, there is a transition from the dry/rainy period, and from August to September the transition between the rainy/dry period. From October to December there is a dry season (Fig. 3). Moura et al. (2020) identified the predictors for rainfall in the eastern sector of Northeast Brazil (ENEB) based on the analysis of canonical correlation. They pointed out that in the months of April and May, the Intertropical Convergence Zone (ITCZ) is the major rain-producing meteorological system. In addition to the ITCZ, the authors highlight the role of the East Wave Disturbances (EWD) and the circulation of sea breezes between June and July (Lyra et al., 2014).

Table 1
Summary of descriptive statistics of monthly rainfall.

Months	Mean	Median	[13]Min	[14]Max	[15]SD	[16]CV	[17]A	[18]K
[1]Jan	99.05	100.20	65.40	135.24	18.06	18.23	−0.02	−0.96
[2]Feb	90.47	87.95	52.59	136.16	22.60	24.98	0.32	−0.84
[3]Mar	129.20	118.95	62.95	191.19	35.14	27.20	0.15	−1.05
[4]Apr	175.16	171.78	90.04	292.63	51.61	29.46	0.22	−0.98
[5]May	210.26	212.83	119.26	306.23	56.20	26.73	−0.07	−1.28
[6]Jun	301.20	284.40	178.10	424.00	74.90	24.88	0.03	−1.48
[7]Jul	229.73	230.96	132.85	331.67	57.64	25.09	−0.03	−1.29
[8]Aug	137.72	138.90	80.20	206.54	37.00	26.87	0.01	−1.16
[9]Sep	73.43	74.06	30.29	101.63	18.87	25.70	−0.28	−0.68
[10]Oct	37.16	37.87	18.13	56.67	10.31	27.73	0.04	−1.03
[11]Nov	26.57	25.80	16.88	42.81	7.37	27.75	0.45	−0.83
[12]Dec	44.62	40.89	27.29	71.03	10.89	24.41	0.49	−0.65

Legend of symbols and acronyms: [1]Jan: January; [2]Feb: February; [3]Mar: March; [4]Apr: April; [5]May: May; [6]Jun: June; [7]Jul: July; [8]Aug: August; [9]Sep: September; [10]Oct: October; [11]Nov: November; [12]Dec: December; [13]Min: Minimum; [14]Max: Maximum; [15]SD: Standard deviation; [16]CV: Coefficient of variation; [17]A: Asymmetry; and [18]K: Kurtosis.

Table 2
Semivariogram model and degree of spatial dependence (DSD) of monthly rainfall patterns.

Months	[13]Mod	[15]C_0	[16]$C_0 + C$	[17]a	[18]R^2	[19]C_0 / ($C_0 + C$)	[20]DSD	Jack-Knifing	
								[21]m	[22]SD
[1]Jan	[14]Gau	120.000	500.000	58,716.520	0.842	0.240	[23]St	0.024	1.177
[2]Feb	Gau	200.000	810.000	56,811.270	0.984	24.691	St	0.000	0.983
[3]Mar	Gau	275.000	1674.000	58,543.320	0.933	16.428	St	−0.015	0.974
[4]Apr	Gau	500.000	4790.000	76,037.000	0.941	10.438	St	−0.011	1.074
[5]May	Gau	550.000	5627.000	88,161.386	0.924	9.774	St	0.011	1.033
[6]Jun	Gau	1100.000	7323.000	60,794.983	0.930	15.021	St	−0.019	0.924
[7]Jul	Gau	1000.000	5282.000	74,824.595	0.916	18.932	St	−0.004	0.995
[8]Aug	Gau	400.000	1794.000	68,935.622	0.917	22.297	St	−0.005	0.952
[9]Sep	Gau	113.000	494.200	60,621.778	0.926	22.865	St	0.003	1.049
[10]Oct	Gau	42.200	261.000	107,906.000	0.945	16.169	St	−0.003	0.998
[11]Nov	Gau	0.100	47.610	9006.664	0.849	0.210	St	0.054	1.106
[12]Dec	Gau	27.600	266.100	86,342.732	0.912	10.372	St	−0.007	0.957

Legend of symbols and acronyms: [1]Jan: January; [2]Feb: February; [3]Mar: March; [4]Apr: April; [5]May: May; [6]Jun: June; [7]Jul: July; [8]Aug: August; [9]Sep: September; [10]Oct: October; [11]Nov: November; [12]Dec: December; [13]Mod: Model; [14]Gau: Gaussian; [15]C_0: Nugget effect; [16]$C_0 + C$: Sill; [17]a: Range (m); [18]R^2: Coefficient of determination; [19]$C_0/(C_0 + C)$: Degree of spatial dependence (%); [20]DSD: Class of the degree of spatial dependence; [21]m: Mean; [22]SD: Standard deviation; and [23]St: Strong.

In the spatial distribution of monthly rainfall, the western portion of the study area shows a significant reduction, due to the topography (Figs. 1 and 2). It is noteworthy that in the extreme west, the Borborema Plateau begins, which extends for 400 km in a straight line, north-south, with coverage in the states of Alagoas, Pernambuco, Paraíba, and Rio Grande do Norte, with direct influence on windward. Recently, Moura et al. (2020) pointed out that the formation of intermediate rainfall windward of the Borborema Plateau was followed by systems such as east waves, breeze circulations, ITCZ, and cold front.

The Atlantic interhemispheric sea surface temperature gradient (AITG) has direct impacts on the NEB coastal rains (Lyra et al., 2017). Dantas et al. (2020) carried out the rain forecast in the state of Paraíba-Brazil, using generalized additive models, they pointed out that there is a persistent influence of the tropical SST (sea surface temperature) patterns on Paraíba's rainfall, with the tropical Atlantic Ocean impacting on rain distribution more effectively than the tropical Pacific Ocean off the Northeastern coast.

3.3. Aquifer distribution, hydrogeology, and groundwater hydrochemistry

Fig. 4 shows the spatial distribution of aquifers (Fig. 4A), hydrogeological (Fig. 4B), and hydrochemistry (Fig. 4C) of groundwater for the study region. There is a greater flow of groundwater on the coast of PE (Fig. 4B), with variation between 10 and 40 $m^3.h^{-1}$ on the south coast, and values of 40–100 and above 100 $m^3.h^{-1}$ for the north coast. This is due to the discharge of groundwater in the Atlantic Ocean, followed by the direct influence of rainfall on the recharge of aquifers on the coast, given that the largest rainfall records are concentrated in this region over the months (Fig. 3).

It was also found that the hydrogeological formation of groundwater on the coast is of the porous type, which justifies the higher flows of groundwater, associated with the higher rainfall records, which provides greater infiltration of rainwater, resulting in recharge and renewal of aquifer waters (Fig. 4B). The quality of groundwater is excellent, regardless of the presence of urban centers, as the extent to which aquifers are recharged, promotes the renewal of water quality.

The western region of the study area has karst and fissure hydrogeological formation, with groundwater quality ranging from medium to improper for the northwest and good quality for the southwest (Fig. 4). This occurrence may be a consequence of the lower rainfall rate in the northwest region and the low degree of massif fracturing, thus characterizing low or no recharge of aquifers in this region (Fig. 3 and Fig. 4).

3.4. Cluster analysis

According to the cluster analysis, using Ward's method (1963), established the Euclidean distances of 0.4 for the months of the year, forming 3 homogeneous (temporal) clusters (Fig. 5A) and 0.05 for the weather stations forming 4 homogeneous (spatial) clusters (Fig. 5B). Cluster 1 (G1) - (79.04 ± 17.18 mm) is composed of the months of December, January, and February. Such months correspond to the transition period in the study area. Cluster 2 (G2) - (197.22 ± 52.09 mm) composed of the months from March to August correspond to the rainy season (Nóbrega et al., 2015). Cluster 3 (G3) - (45.72 ± 12.18 mm) refers to the dry period, formed by the months of September, October, and November (Fig. 5A). Teodoro et al. (2016), highlight that the cluster analysis is an efficient statistic in the characterization of the dry, rainy months and intermediaries, as pointed out in this study.

From the clusters formed by the weather stations (Fig. 5B), a spatial map of the clusters represented in Fig. 6 was generated. Cluster 1 refers to the southern region, cluster 2 is located on the coast of the state of Pernambuco, while clusters 3 and 4 are located to the north of the study area.

The spatial dynamics of the clusters formed by the cluster analysis provided an efficient characterization of the distribution of weather stations, enabling a better spatial understanding of the dynamics of the rains, as well as their uniformity (Fig. 6). Based on the kriging maps represented in Fig. 3, the northern and southern regions register lower rainfall due to higher altitudes (Fig. 1), while

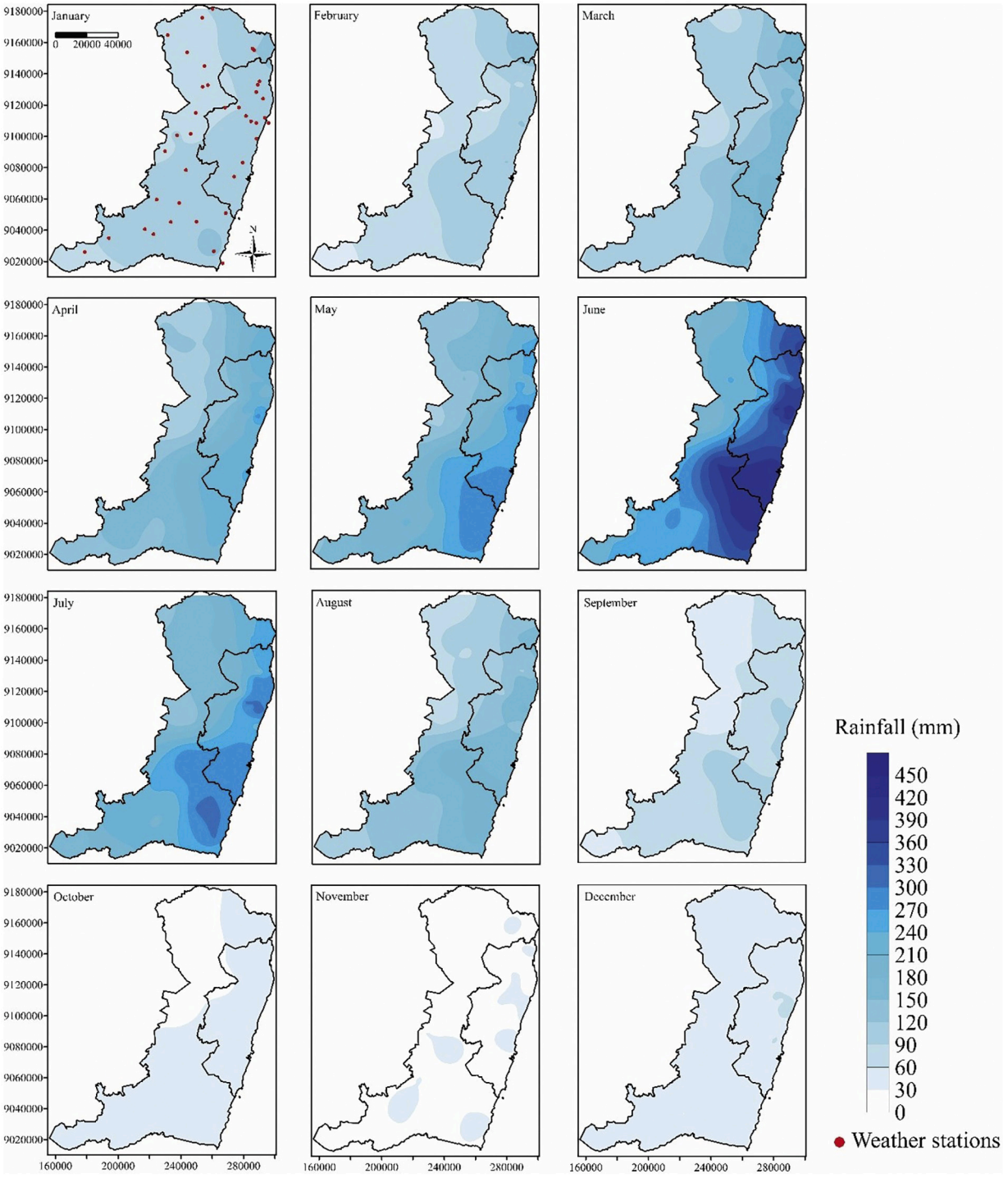

Fig. 3. Maps of rainfall kriging (mm) for the months from January to December in the period 2000–2019 in the mesoregions of Zona da Mata and Recife Metropolitan Region in the State of Pernambuco, Brazil.

stations close to the state's coast register higher rainfall because they are closer to sea level (Fig. 1) and have a direct influence on ocean air masses. Thus, it is possible to prioritize the installation of future stations in regions of greater precipitation, given the impacts that the rains cause on the coast of the state, which would allow obtaining more concise data, for future studies that seek to characterize more accurately the impacts of rainfall on the coast of the state of Pernambuco.

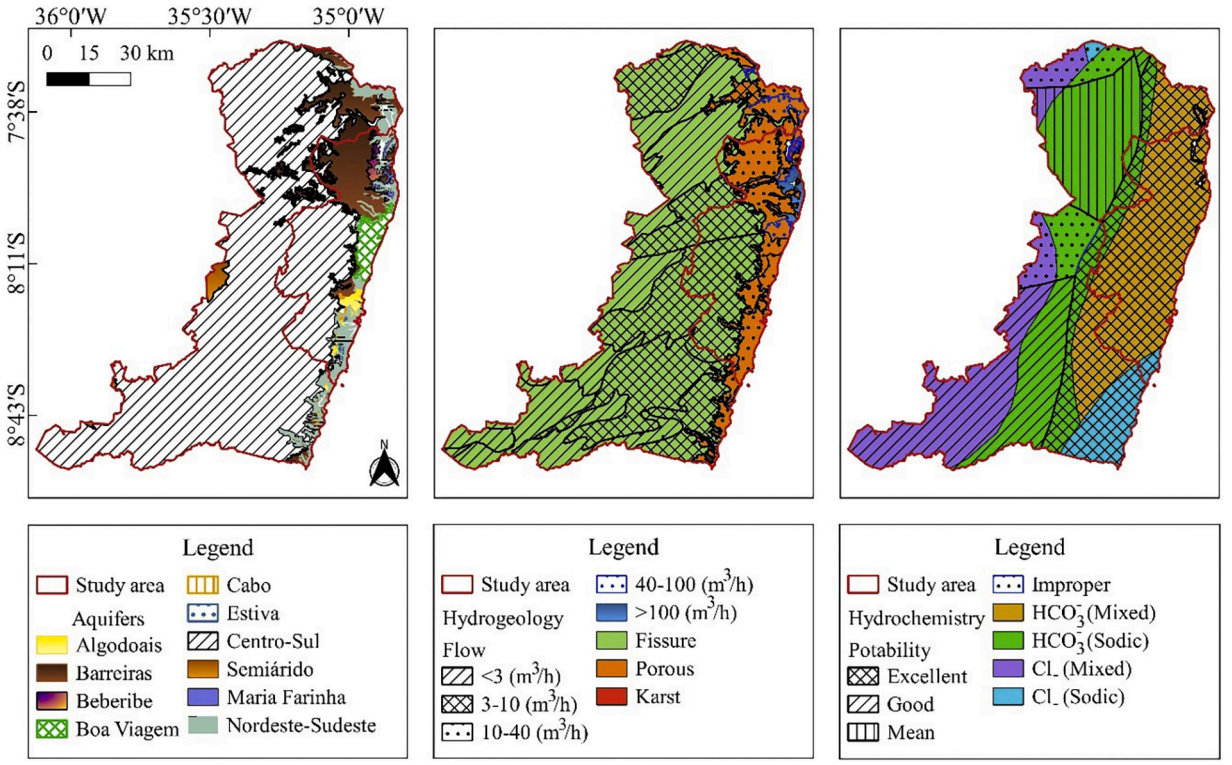

Fig. 4. Maps of the distribution of aquifers (A), hydrogeology (B), and hydrochemistry (C) of groundwater.

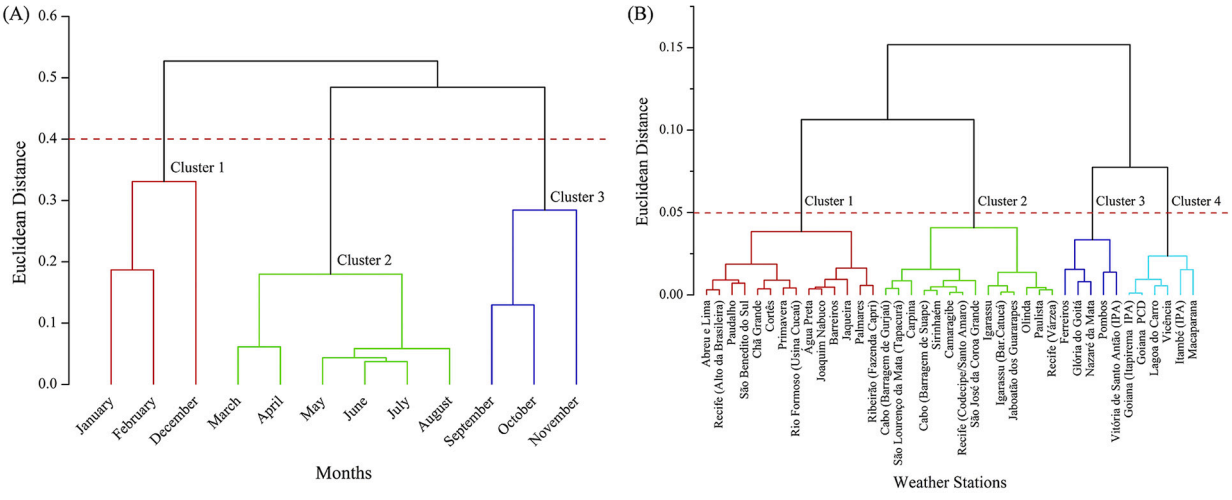

Fig. 5. Analysis of clustering by the dendrogram, for the average of the months from January to December (A) and for the weather stations (B) of the time series from 2000 to 2019.

3.5. Rainfall impact on the urban area

According to the IBGE, the Metropolitan Region of Recife is among the 10 largest urban centers in Brazil, with an unbridled expansion of industries, which promotes an increase in population and the formation of small centers in the metropolis. Another critical point is the high flow of tourists throughout the year, especially at the carnival event and the June party, which directly impacts the production of waste and urban pollution.

Faced with these problems, there is still a deficiency in urban sanitation, which in the period of heavy rains (April–August), with an emphasis on the months of June and July, occurs floods and floods in the metropolitan center, generating socioeconomic losses, in

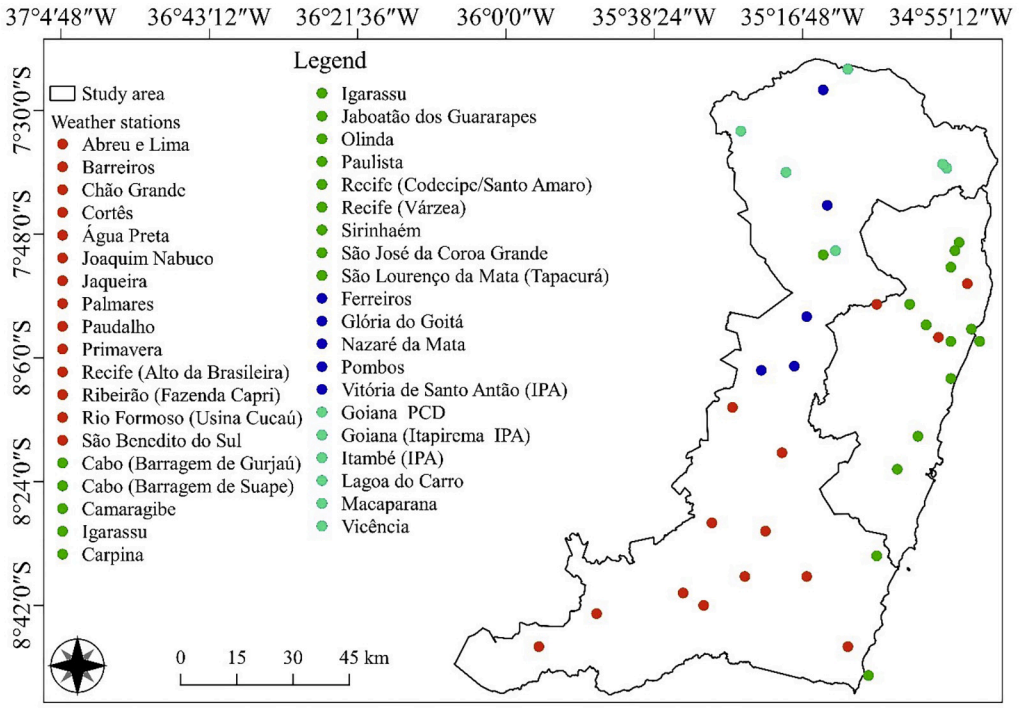

Fig. 6. Map of the distribution of clusters generated in the cluster analysis of weather stations (Fig. 5B) in the study region.

addition to drowning deaths. Therefore, kriging maps become fundamental in urban planning and, thus, it makes it possible to establish a strategy in urban management and public policies in the great centers of the Pernambuco coast, mainly in the metropolitan mesoregion of Recife, which can be used in the evaluation of other urban regions in Brazil.

4. Conclusions

The Gaussian transitive theoretical model satisfactorily represents the spatial analysis of rainfall in the coastal region of the state of Pernambuco - Brazil. The kriging spatial interpolation method provides consistent rainfall spatialization on the Pernambuco coast, with an emphasis on the extreme west which is influenced by the Borborema Plateau, which allows the assessment of rainfall dynamics and the creation of socioeconomic strategies to minimize impacts on the period of heavy rains and great floods; besides, it makes it possible to associate the dynamics and quality of groundwater on the coast with an emphasis on its suitability for human consumption.

The cluster analysis allows the temporal identification of three homogeneous groups of rains, in the dry, rainy, and transition months. Regarding the spatial variation, four homogeneous rainfall groups were identified for the southern, northern, and coastal regions of the state of PE.

Rainfall has a direct influence on the recharge of local aquifers, based on the hydrogeological and hydrochemical analysis of groundwater via remote sensing of the present study. There is a need for in situ studies based on the hydrogeology and hydrochemistry of groundwater and to associate urban factors that can impact water dynamics. In our study, we highlight only the rainfall factor, with the need to assess the other factors (septic tank, pollution of local rivers and lakes, pollution of the Atlantic coast that bathes the study region, and others).

Spatial modeling via kriging maps is fundamental in urban planning and, thus, makes it possible to establish strategies in urban management and public policies in large urban centers in Brazil and the world. The established geostatistical models can be used to assess precipitation in large centers in Brazil and the world.

This research will assist in the formulation of public policies for disaster risk management and assist the next public and private investments in the Pernambuco coast, given the 20-year historical series, and by updating the knowledge of rainfall patterns. In the rainy season, problems with flooding on the coast of Pernambuco are common, especially in the metropolitan region of Recife.

Declaration of Competing Interest

The authors declare that they have no known competing financial interests or personal relationships that could have appeared to influence the work reported in this paper.

Acknowledgments

To the *Programa de Pós-Graduação em Engenharia Agrícola* (PGEA) and the *Grupo de Pesquisa em Ambiência* (GPESA) of the *Universidade Federal Rural de Pernambuco* (UFRPE) for the support and supply of equipment for the development of this research. The *Coordenação de Aperfeiçoamento de Pessoal de Nível Superior* (CAPES - Finance Code 001), the *Fundação de Amparo à Ciência e Tecnologia do Estado de Pernambuco* (FACEPE - APQ-0215-5.01/10 and FACEPE - APQ-1159-1.07/14), and the *Conselho Nacional de Desenvolvimento Científico e Tecnológico* (CNPq), for the funding of scholarships and productivity (CNPq - 304060/2016-0, and 309421/2018-7). The fourth author would like to thank CNPq's Research Productivity scholarship level 2 under case number (CNPq - 309681/2019-7). The authors would also like to thank the editor and anonymous reviewer for their helpful comments on an earlier draft of this manuscript.

References

Alvares, C.A., Stape, J.L., Sentelhas, P.C., de Moraes Gonçalves, J.L., Sparovek, G., 2013. Köppen's climate classification map for Brazil. Meteorol. Z. 22 (6), 711–728. https://doi.org/10.1127/0941-2948/2013/0507.

APAC, 2020. Climatologia [online]. Available at: https://www.apac-homo.pe.gov.br/climatologia/519-climatologia [Accessed November 18, 2020].

Arowolo, A.O., Bhowmik, A.K., Qi, W., Deng, X., 2017. Comparison of spatial interpolation techniques to generate high - resolution climate surfaces for Nigeria. Int. J. Climatol. 37, 179–192. https://doi.org/10.1002/joc.4990.

Baklanov, A., Molina, L.T., Gauss, M., 2016. Megacities, air quality and climate. Atmos. Environ. 126, 235–249. https://doi.org/10.1016/j.atmosenv.2015.11.059.

Beck, H.E., Zimmermann, N.E., McVicar, T.R., Vergopolan, N., Berg, A., Wood, E.F., 2018. Present and future Köppen-Geiger climate classification maps at 1-km resolution. Scientific Data 5, 180214. https://doi.org/10.1038/sdata.2018.214.

Brito, T.T., Oliveira-Júnior, J.F., Lyra, G.B., Gois, G., Zeri, M., 2017. Multivariate analysis applied to monthly rainfall over Rio de Janeiro state, Brazil. Meteorog. Atmos. Phys. 129 (5), 469–478. https://doi.org/10.1007/s00703-016-0481-x.

Cambardella, C.A., Moorman, T.B., Novak, J.M., Parkin, T.B., Karlen, D.L., Turco, R.F., Konopka, A.E., 1994. Field-scale variability of soil properties in Central Iowa soils. Soil Sci. Soc. Amsterdam J. 58, 1501–1511. https://doi.org/10.2136/sssaj1994.03615995005800050033x.

Campling, P., Gobin, A., Feyen, J., 2001. Temporal and spatial rainfall analysis across a humid tropical catchment. Hydrol. Process. 15 (3), 359–375. https://doi.org/10.1002/hyp.98.

Core Team, R., 2019. R: A Language and Environment for Statistical Computing. R Foundation for Statistical Computing.

Costa, M.S., Oliveira-Júnior, J.F., Santos, P.J., Correia Filho, W.L.F., Gois, G., Blanco, C.J.C., Teodoro, P.E., Silva Junior, C.A., Santiago, B.D., Souza, E.O., Jardim, A. M.R.F., 2021. Rainfall extremes and drought in Northeast Brazil and its relationship with El Niño–southern oscillation. Int. J. Climatol. 41, E2111–E2135. https://doi.org/10.1002/joc.6835.

Courty, L.G., Rico-Ramirez, M.Á., Pedrozo-Acuña, A., 2018. The significance of the spatial variability of rainfall on the numerical simulation of urban floods. Water 10 (2), 207. https://doi.org/10.3390/w10020207.

CPRM, 2007. Mapa de Domínios/Subdomínios Hidrogeológicos do Brasil 1:2.500.000 [online]. Available at: http://www.cprm.gov.br/publique/Hidrologia/Mapas-e-Publicacoes/Mapa-de-Dominios%7CSubdominios-Hidrogeologicos-do-Brasil-1%3A2.500.000-632.html [Accessed 1 July 2020].

Dai, Q., Zhu, X., Zhuo, L., Han, D., Liu, Z., Zhang, S., 2020. A hazard-human coupled model (HazardCM) to assess city dynamic exposure to rainfall-triggered natural hazards. Environ. Model Softw. 104684. https://doi.org/10.1016/j.envsoft.2020.104684.

Dantas, L.G., dos Santos, C.A., Olinda, R.A.D., de Brito, J.I., Santos, C.A., Martins, E.S., Brunsell, N.A., 2020. Rainfall prediction in the state of Paraíba, northeastern Brazil using generalized additive models. Water 12 (9), 2478. https://doi.org/10.3390/w12092478.

Deutsch, C.V., Journel, A.G., 1998. GSLIB Geostatistical Software Library and User's Guide, Second ed. Oxford University Press, New York, p. 369.

England, E.J., Sparks, A., Robinson, M.D., 1989. Geo—EAS (geostatistical environmental assessment software). Environ. Softw. 4 (2), 70–75. https://doi.org/10.1016/0266-9838(89)90033-6.

Gois, G., Delgado, R.C., de Oliveira Júnior, J.F., 2015. Modelos teóricos transitivos aplicados na interpolação espacial do Standardized Precipitation Index (SPI) para os episódios de El Niño forte no Estado do Tocantins, Brasil. Irriga 20 (2), 371–387. https://doi.org/10.15809/irriga.2015v20n2p371.

Gois, G., Oliveira-Júnior, J.F., Silva Junior, C.A., Sobral, B.S., Bodas Terassi, P.M., Junior, A.H.S.L., 2020. Statistical normality and homogeneity of a 71-year rainfall dataset for the state of Rio de Janeiro—Brazil. Theor. Appl. Climatol. 141 (3), 1573–1591. https://doi.org/10.1007/s00704-020-03270-9.

GOLDEN SOFTWARE, 2010. Surfer for Windows Version 9.0. Colorado, Golden, p. 66.

Haris, H., Chow, M.F., Sidek, L.M., 2017, July. Spatial variability of rainfall in urban catchment. In: Global Civil Engineering Conference. Springer, Singapore, pp. 1075–1086. https://doi.org/10.1007/978-981-10-8016-6_76.

IBGE, 2018. Levantamento Hidrogeologico [online]. Available at: http://geoftp.ibge.gov.br/informacoes_ambientais/geologia/levantamento_hidrogeologico_e_hidroquimico/vetores/regionais/?fbclid=IwAR2TbZ0MFLJEUHKjVWv6IbgPkqReC2vN7H6tMg3R_3AI01ndqVTgh3mr000 [Accessed September 18, 2020].

IBGE, 2020a. CONHEÇA CIDADES E ESTADOS DO BRASIL [online]. Available at: https://cidades.ibge.gov.br/ [Accessed September 23, 2020].

IBGE, 2020b. Hidroquímica subterrânea [online]. Available at: https://www.ibge.gov.br/geociencias/informacoes-ambientais/geologia/15824-hidrogeologia.html?=&t=downloads [Accessed September 19, 2020].

INDE, 2013. CONHEÇA CIDADES E ESTADOS DO BRASIL [online]. Available at: http://www.metadados.inde.gov.br/geonetwork/srv/br/metadata.show.embedded?uuid=3ec60e4f-85ea-4ba7-a90c-734b57594f90 [Accessed October 05, 2020].

Jardim, A.M.R.F., Araújo Júnior, G.N., Silva, M.J., Morais, J.E.F., Silva, T.G.F., 2017. Estimativas de perda de solo por erosão hídrica para o município de Serra Talhada, PE. J. Environ. Anal. Progr. 186–193. https://doi.org/10.24221/jeap.2.3.2017.1416.186-193.

Jardim, A.M.R.F., Queiroz, M.G., Araújo Júnior, G.N., Silva, M.J., Silva, T.G.F., 2019. Estudos climáticos do número de dias de precipitação pluvial para o município de Serra Talhada-PE. Rev. Engenharia Agric. 27 (4), 330–337. https://doi.org/10.13083/reveng.v27i4.875.

Javari, M., 2017a. Geostatistical modeling to simulate daily rainfall variability in Iran. Cogent Geosci. 3 (1), 1416877. https://doi.org/10.1080/23312041.2017.1416877.

Javari, M., 2017b. Spatial variability of rainfall trends in Iran. Arab. J. Geosci. 10 (4), 78. https://doi.org/10.1007/s12517-017-2857-8.

Kamruzzaman, M., Beecham, S., Metcalfe, A.V., 2011. Non-stationarity in rainfall and temperature in the Murray Darling basin. Hydrol. Process. 25 (10), 1659–1675. https://doi.org/10.1002/hyp.7928.

Kamruzzaman, M., Beecham, S., Metcalfe, A.V., 2017. Changing patterns in rainfall extremes in South Australia. Theor. Appl. Climatol. 127 (3), 793–813. https://doi.org/10.1007/s00704-015-1667-8.

Kitanidis, P.K., 1997. Introduction to Geostatistics: Applications in Hydrogeology. Cambridge University Press.

Kite, G., 1988. Frequency and Risk Analyses in Hydrology. Water Resourcers Publications, Littleton, p. 257.

Lima, A.O., Lyra, G.B., Abreu, M.C., Oliveira-Júnior, J.F., Zeri, M., Cunha-Zeri, G., 2021. Extreme rainfall events over Rio de Janeiro state, Brazil: characterization using probability distribution functions and clustering analysis. Atmos. Res. 247, 105221. https://doi.org/10.1016/j.atmosres.2020.105221.

Lopes, I., Silva, M.V.D., de Melo, J.M., Montenegro, A.A.D.A., Pandorfi, H., 2020. Geostatistics applied to the environmental mapping of aviaries. Rev. Brasil. Engenharia Agríc. Ambient. 24 (6), 409–414. https://doi.org/10.1590/1807-1929/agriambi.v24n6p409-414.

Lyra, G.B., OliveiraJúnior, J.F., Zeri, M., 2014. Cluster analysis applied to the spatial and temporal variability of monthly rainfall in Alagoas state, northeast of Brazil. Int. J. Climatol. 34 (13), 3546–3558. https://doi.org/10.1002/joc.3926.

Lyra, G.B., Oliveira-Júnior, J.F., Gois, G., Cunha-Zeri, G., Zeri, M., 2017. Rainfall variability over Alagoas under the influences of SST anomalies. Meteorog. Atmos. Phys. 129 (2), 157–171. https://doi.org/10.1007/s00703-016-0461-1.

Medeiros, E.S.D., Lima, R.R.D., Olinda, R.A.D., Santos, C.A.C.D., 2019. Modeling spatiotemporal rainfall variability in Paraíba, Brazil. Water 11 (9), 1843. https://doi.org/10.3390/w11091843.

Moura, G.B.A., de Brito, J.I.B., de Assis, F., de Sousa, S., Cavalcanti, E.P., da Silva, J.L.B., Nascimento, P.M.O.L., 2020. Identificação de preditores para as chuvas do setor leste do Nordeste do Brasil utilizando análise de correlação canônica. Rev. Brasil. Geogr. Física 13 (04), 1463–1482. https://doi.org/10.26848/rbgf.v13.4.p1463-1482.

Nóbrega, R.S., Farias, R.F.D.L., Santos, C.A.C.D., 2015. Variabilidade temporal e espacial da precipitação pluviométrica em Pernambuco através de índices de extremos climáticos. Rev. Brasil. Meteorol. 30 (2), 171–180. https://doi.org/10.1590/0102-778620130624.

Oliveira-Júnior, J.F., Gois, G., da Silva, E.B., Teodoro, P.E., Johann, J.A., Junior, C.A.S., 2019. Non-parametric tests and multivariate analysis applied to reported dengue cases in Brazil. Environ. Monit. Assess. 191 (7), 473. https://doi.org/10.1007/s10661-019-7583-0.

Peña-Angulo, D., Nadal-Romero, E., González-Hidalgo, J.C., Albaladejo, J., Andreu, V., Barhi, H., Campo-Bescós, M.A., 2020. Relationship of weather types on the seasonal and spatial variability of rainfall, runoff, and sediment yield in the Western Mediterranean Basin. Atmosphere 11 (6), 609. https://doi.org/10.3390/atmos11060609.

QGIS Development Team, 2020. Quantum Geographic Information System Version 3.12. Open Source Geospatial Foundation Project. https://qgis.org/en/site/.

Rahman, M.H., Matin, M.A., Salma, U., 2018. Analysis of precipitation data in Bangladesh through hierarchical clustering and multidimensional scaling. Theor. Appl. Climatol. 134 (1–2), 689–705. https://doi.org/10.1007/s00704-017-2319-y.

Ramos, A.M., Cortesi, N., Trigo, R.M., 2014. Circulation weather types and spatial variability of daily precipitation in the Iberian Peninsula. Front. Earth Sci. 2, 25. https://doi.org/10.3389/feart.2014.00025.

Santos, C.A.G., Brasil Neto, R.M., da Silva, R.M., Costa, S.G.F., 2019. Cluster analysis applied to spatiotemporal variability of monthly precipitation over paraíba state using tropical rainfall measuring mission (TRMM) data. Remote Sens. 11 (6), 637. https://doi.org/10.3390/rs11060637.

Santos, Y., Silva, E., Oliveira Júnior, J.F., Santos, P., Costa, L.M., 2018. Diagnóstico da morbidade e mortalidade dos casos de leptospirose no Nordeste brasileiro entre 2000 a 2015. Enciclopédia Biosf. 15 (27) https://doi.org/10.18677/EnciBio_2018A34.

Sarangi, A., Cox, C.A., Madramootoo, C.A., 2005. Geostatistical methods for prediction of spatial variability of rainfall in a mountainous region. Trans. ASAE 48 (3), 943–954. https://doi.org/10.13031/2013.18507.

Serra, A., Merc, B., Vendrell, R., 2016. Automatic weather stations network (XEMA) of the Meteorological Service of Catalonia (SMC). In: WMO Technical Conference on Meteorological and Environmental Instruments and Methods of Observation (CIMO TECO 2016): Ensuring Sustained High-Quality Meteorological Observations from Sea, Land and Upper Atmosphere in a Changing World. WMO. URL: https://library.wmo.int/index.php?lvl=notice_display&id=19676#XEWdHvZ7m70.

Silva, F.F., dos Santos, F.D.A., dos Santos, J.M., 2020b. Índice de anomalia de chuva (IAC) aplicado ao estudo das precipitações no município de caridade, Ceará, Brasil. Rev. Brasil. Climatol. 27 https://doi.org/10.5380/abclima.v27i0.74274.

Silva, J.L.B., Albuquerque Moura, G.B., Silva, M.V., Souza, R.V., Guedes, P.M.O.L., França, È.F., Hozana, A., 2020a. Inferência Exploratória de Dados Espaço-Temporal da Precipitação Pluviométrica no Nordeste Brasileiro. Rev. Brasil. Geogr. Física 13 (05), 2019–2036. https://doi.org/10.26848/rbgf.v13.5.p2019-2036.

Silva, M.J., Queiroz, M.G., Jardim, A.M.R.F., Araújo Júnior, G.N., Silva, T.G.F., 2018. Gradientes pluviométricos do estado de Pernambuco: Uma análise do Litoral ao Semiárido. Rev. Engenharia Agric. 26 (3), 240–249. https://doi.org/10.13083/reveng.v26i3.889.

Silva, M.V., Almeida, G.L.P., Batista, P.H.D., Pandorfi, H., Almeida Macêdo, G.A.P., Mesquita, M., Silva, R.A.B., 2019. Variabilidade Espacial dos Atributos Físicos do Solo em Área Cultivada com Palma Forrageira Resistente a Cochonilha do Carmim no Semiárido Nordestino. Anu. Inst. Geocienc. 42 (4), 39–45. https://doi.org/10.11137/2019_4_39_45.

Silva, M.V., Pandorfi, H., Almeida, G.L.P., Jardim, A.M.R.F., Batista, P.H.D., Silva, R.A.B., Moraes, A.S., 2020c. Spatial variability and exploratory inference of abiotic factors in barn compost confinement for cattle in the semiarid. J. Therm. Biol. 94, 102782. https://doi.org/10.1016/j.jtherbio.2020.102782.

Sivakumar, B., Woldemeskel, F.M., Vignesh, R., Jothiprakash, V., 2019. A correlation–scale–threshold method for spatial variability of rainfall. Hydrology 6 (1), 11. https://doi.org/10.3390/hydrology6010011.

Teodoro, P.E., Oliveira-Júnior, J.F., Cunha, E.R., Correa, C.C.G., Torres, F.E., Bacani, V.M., Ribeiro, L.P., 2016. Cluster analysis applied to the spatial and temporal variability of monthly rainfall in Mato Grosso do Sul state, Brazil. Meteorog. Atmos. Phys. 128 (2), 197–209. https://doi.org/10.1007/s00703-015-0408-y.

Terassi, P.M.B., Oliveira-Júnior, J.F., Gois, G., Júnior, A.C.O., Sobral, B.S., Biffi, V.H.R., Vijith, H., 2020. Rainfall and erosivity in the municipality of Rio de Janeiro-Brazil. Urban Clim. 33, 100637. https://doi.org/10.1016/j.uclim.2020.100637.

Thom, H.C.S., 1966. Same Methods of Climatological Analyses. World Meteorological Organization-WMO, Geneva, p. 53 (Technical Note, 81).

Tobar, V., Wyseure, G., 2017. Seasonal rainfall patterns classification, relationship to ENSO and rainfall trends in Ecuador. Int. J. Climatol. 38 (4), 1808–1819. https://doi.org/10.1002/joc.5297.

Uele, D.I., Lyra, G.B., Oliveira Júnior, J.F.D., 2017. Variabilidade Espacial e Intranual das Chuvas na Região Sul de Moçambique, África Austral. Rev. Brasil. Meteorol. 32 (3), 473–484. https://doi.org/10.1590/0102-77863230013.

Vauclin, M., Vieira, S.R., Vachaud, G., Nielsen, D.R., 1983. The use of Cokriging with limited field soil observations 1. Soil Sci. Soc. Am. J. 47 (2), 175–184. https://doi.org/10.2136/sssaj1983.03615995004700020001x.

Vessia, G., Di Curzio, D., Chiaudani, A., Rusi, S., 2020. Regional rainfall threshold maps drawn through multivariate geostatistical techniques for shallow landslide hazard zonation. Sci. Total Environ. 705, 135815. https://doi.org/10.1016/j.scitotenv.2019.135815.

Ward, J.H., 1963. Hierarchical grouping to optimize an objective function. J. Am. Stat. Assoc. 58 (301), 236–244. https://doi.org/10.1080/01621459.1963.10500845.

Warrick, A.W., Nielsen, D.R., 1980. Spatial variability of soil physical properties in the field. In: Hillel, D. (Ed.), Applications of Soil Physics, vol. 2. Academic, New York, pp. 319–344.

Wodaje, G.G., Eshetu, Z., Argaw, M., 2016. Temporal and spatial variability of rainfall distribution and evapotranspiration across altitudinal gradient in the Bilate River watershed, southern Ethiopia. Afr. J. Environ. Sci. Technol. 10 (6), 167–180. https://doi.org/10.5897/AJEST2015.2029.

Yilmaz, A.G., Imteaz, M.A., Perera, B.J.C., 2016. Investigation of non-stationarity of extreme rainfalls and spatial variability of rainfall intensity–frequency–duration relationships: a case study of Victoria, Australia. Int. J. Climatol. 37 (1), 430–442. https://doi.org/10.1002/joc.4716.